Voltage-controlled magnetic anisotropy and voltage-induced Dzyaloshinskii-Moriya interaction change at the epitaxial Fe(001)/MgO(001) interface engineered by Co and Pd atomic-layer insertion

Joko Suwardy,[1] Kohei Nawaoka,[1] Jaehun Cho,[1] Minori Goto,[1,2] Yoshishige Suzuki,[1,2] and Shinji Miwa[1,2,3,*]

[1]*Graduate School of Engineering Science, Osaka University, Toyonaka, Osaka 560-8531, Japan*

[2]*Center for Spintronics Research Network (CSRN), Osaka University, Toyonaka, Osaka 560-8531, Japan*

[3]*The Institute for Solid State Physics, The University of Tokyo, Kashiwa, Chiba 277-8581, Japan*

(Received 4 July 2018; revised manuscript received 7 September 2018; published 23 October 2018)

We fabricated epitaxial multilayers with Co and Pd atomic-layer insertion at Fe(001)/MgO(001) interface and systematically investigated voltage-controlled magnetic anisotropy (VCMA) and voltage-induced interfacial Dzyaloshinskii-Moriya interaction (iDMI) change. The VCMA and iDMI change was characterized by spin-wave spectroscopy. We found that the VCMA was increased by Co and Pd insertions to -180 fJ/Vm in the Fe/Co/Pd/MgO system. We also found a large voltage-induced iDMI change of 65 fJ/Vm. The postannealing dependence of the VCMA and iDMI change was also characterized to investigate the influence of the change in chemical ordering around the MgO interface.

DOI: 10.1103/PhysRevB.98.144432

I. INTRODUCTION

Spin-transfer torque-induced magnetization switching has become a common way to switch the magnetization direction in nonvolatile magnetoresistive random-access memory (MRAM) devices [1,2]. However, the energy required to switch magnetization directions by the spin-transfer effect is large at $\sim 10^7$ times higher than the Landauer limit of $k_B T \ln 2$, where k_B is the Boltzmann constant [3]. This energy dissipation occurs by Joule heating caused by the electron flow. Consequently, a new control technique for magnetization is necessary. Voltage-controlled magnetic anisotropy (VCMA) in ferromagnetic metals [4,5], a kind of magneto-electric effect, permits spin manipulation and thus enables the construction of ultralow-power high-density MRAM [6]. The VCMA can be observed in Fe-MgO-based magnetic tunnel junctions (MTJs) [7]. Furthermore, purely electronic VCMA, as demonstrated by VCMA-induced precessional magnetization switching [8–10] and ferromagnetic resonance excitation [11,12], showed a high-speed response (<0.1 ns), indicating the feasibility of voltage-driven MRAM. However, the enhancement of electronic VCMA efficiency remains a challenge.

Interface engineering is a promising approach to improve VCMA efficiency, because the modulation of magnetic anisotropy arises from electronic modification at the interface of the ferromagnet and a dielectric layer. First-principles studies have reported large enhancements in VCMA efficiency by inserting heavy metals at the interface or surface [13,14]. Recently, Pt (Ref. [15]) and Ir (Ref. [16]) insertion at the Fe/MgO interface were reported to enhance the VCMA effect, which may correspond to the large spin-orbit interaction coefficients of 5d metals. Moreover, in the $L1_0$–FePt system, VCMA can be explained by both voltage inductions of the orbital magnetic moment and the magnetic dipole T_z term (electric quadrupole) [15]. However, these two contributions partially cancel each other, yielding relatively low VCMA efficiency. Other than 5d metals, the insertion of the 4d metal Pd has also been reported. A sputter-deposited Co/Pd/MgO system showed the VCMA efficiencies of -66 fJ/Vm (Ref. [17]) and 1600 fJ/Vm (Ref. [18]) at room temperature and 10 K, respectively. Previously, it was reported that the orbital magnetic moment and magnetic dipole T_z term in an FePd alloy could be modified through changes in chemical ordering [19]. Therefore, alloying of the interface, which corresponds to changing the chemical order, attached to the MgO layer may be one approach to achieve a high VCMA efficiency. It is thus interesting to characterize VCMA under Pd layer insertion at the Fe(Co)/MgO interface and the postannealing dependence of the VCMA.

In this study, we investigate systematically Co and/or Pd atomic-layer insertion at Fe/MgO interfaces using a well-defined epitaxial multilayered system. We characterized the VCMA efficiency by propagating spin-wave spectroscopy. In order to investigate the influence of chemical order on the VCMA efficiency, the postannealing dependence was also studied. In this work, we characterized not only VCMA effect but also voltage-induced changes in the interfacial Dzyaloshinskii-Moriya interaction (iDMI) [20,21]. Because the voltage-induced iDMI change breaks time-reversal symmetry in systems, it can be useful for stable VCMA-induced magnetization switching [22] and the control of chiral magnetic structures [23].

II. EXPERIMENTAL

The sample structure used in this study is illustrated in Fig. 1(a). Multilayers consisting of MgO(001) buffers (5 nm)/body-centered cubic (bcc)-V (001) (20 nm)/bcc-Fe(001) (20 nm)/Co(t_{Co})/Pd(t_{Pd})/MgO(001) barriers (5 nm) were grown onto NaCl-type single-crystal MgO(001) substrates by

*miwa@issp.u-tokyo.ac.jp

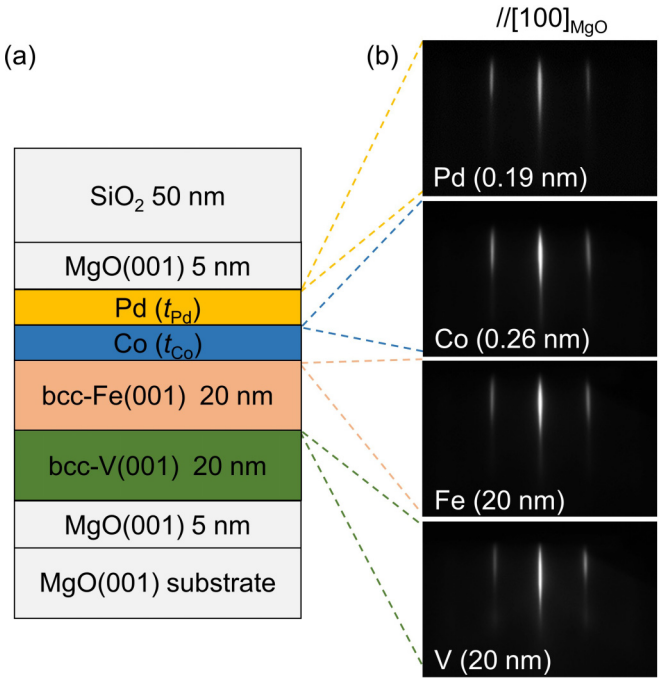

FIG. 1. (a) Schematic of the sample structure. Thickness of Co (t_{Co}) and Pd (t_{Pd}) are varied from 0 to 0.52 nm (0–4 ML) and 0 to 0.95 nm (0–5 ML), respectively. (b) Reflection high-energy electron diffraction images from the top surfaces of the V, Fe, Co, and Pd layers, where the incident beam is aligned with the [100] direction of the MgO(001) substrate.

the electron-beam deposition technique of molecular-beam epitaxy under ultrahigh vacuum (base pressure $\sim 10^8$ Pa). A common method to characterize VCMA involves the use of a MTJ structure, in which the ferromagnetic layer thickness is typically 1–2 nm. However, to study VCMA with various thicknesses, the spin-wave spectroscopy is advantageous because it can be applicable to materials with wide ranges of interfacial PMA and DMI [20]. Notably, VCMA and iDMI change are determined only by the condition of the interface layer attached to the MgO layer and are independent of the ferromagnetic layer thickness. While a relatively thick ferromagnetic layer (20 nm) is employed for spin-wave spectroscopy to obtain high signal-to-noise ratio, the condition and materials obtained can be transferred to a more realistic structure for MRAM device. The MgO substrate was annealed at 800 °C for 10 min before the multilayer deposition. To prevent carbon diffusion from the MgO substrate surface [24], the MgO(001) buffer layer was grown at 250 °C. After cooling, the V buffer and Fe layers were deposited at room temperature. To obtain a clean and flat surface, the V buffer layer and Fe layer were postannealed at 500 °C for 30 min and 250 °C for 15 min, respectively. Afterward, 0–0.52 nm [~0–4 monolayers (MLs)] of Co and 0–0.95 nm (~0–5 MLs) of Pd were deposited without heating the substrate. The Co layer is assumed to grow as a bcc structure with lattice parameter $a = 0.26$ nm on top of bcc-Fe, while the Pd layer has a fcc-structure with lattice constant of 0.389 nm. All the layers with various thicknesses were prepared on the same wafer by using a position-controlled linear shutter during deposition. With these thickness variations, we can investigate the interfaces of Fe/MgO, Co/MgO, Fe/Pd/MgO, and Co/Pd/MgO. After the MgO barrier deposition, the multilayer was removed from vacuum. A 50-nm-thick SiO_2 layer was deposited by sputtering as an additional dielectric layer. Figure 1(b) shows images obtained by reflection high-energy electron diffraction of the V, Fe, Co, and Pd layers. Sharp streak patterns are observed in all layers, indicating the formation of epitaxial and flat interfaces at each layer. The 0.26-nm Co (~2 ML) and 0.19-nm Pd (~1 ML) layers are confirmed to have grown coherently onto the bcc-Fe(001) surface.

The characterizations of VCMA and iDMI changes in the multilayers depicted in Fig. 1 were conducted by spin-wave spectroscopy. Figure 2(a) shows the top view of the spin-wave device with the measurement geometry. By using electron-beam lithography and Ar ion milling, the multilayer film was patterned into a rectangular shape ($100 \times 400\ \mu$m) with the long axis parallel to the Fe[100] direction. Two antennas (short-circuit coplanar waveguide) composed of Cr (5 nm)/Au (200 nm) films were fabricated parallel to the Fe[100] direction through a lift-off process. An in-plane magnetic field was applied in the y direction to excite the magnetostatic surface spin wave (MSSW). The two individual antennas separated by 10 μm were designed to excite and detect the spin waves in the $\pm x$ direction with the wave number (k) of 1.2 μm^{-1}. The inset of Fig. 2(a) depicts the antenna that consists of a signal line (2 μm) and two ground lines (1 μm) with gaps of 1 μm, and an intermediate gate electrode between the antennas. The voltage is applied to the Fe ferromagnetic layer, which is schematically depicted in the left-hand-side inset. The MSSW in the device was analyzed by measuring the S parameters using a vector network analyzer (VNA) with an applied radio-frequency power of −15 dBm (32 μW) and a bandwidth of 1 kHz. An intermediary gate electrode was placed between the two antennas; all are connected to the same ground via bias-tee. To investigate the electric-field-induced changes of the interfacial magnetic anisotropy and Dzyaloshinskii-Moriya interactions, that is, the VCMA and iDMI change, a bias voltage (V_{dc}) was applied during the spin-wave measurements. It was previously reported that changes in the chemical order of ferromagnetic materials around interfaces with MgO may influence the VCMA [15]. To observe this, we also performed the spin-wave measurements with postannealed devices. The postannealing of the spin-wave device was conducted for 30 min at 200–300 °C under high vacuum ($<4 \times 10^{-4}$ Pa).

Figure 2(b) shows the typical spin-wave resonant frequency (f_R) under different external magnetic fields (H_{ext}) for the Fe/Co (0.52 nm)/Pd (0.19 nm)/MgO sample. The frequency is determined from the peak position of the $|S_{11}|$ spectrum. For instance, a spectrum under $\mu_0 H_{ext} = 40$ mT is depicted in Fig. 2(b) inset. In this case, no bias voltage was applied ($V_{dc} = 0$). To analyze the fourfold crystalline anisotropy ($\mu_0 H_{cry}$) and the interfacial perpendicular anisotropy field ($\mu_0 H_{int}$), we fitted the resonant frequency (f_R) by using the following equation [20,25]:

$$f_R = -\frac{\gamma_0 \mu_0}{2\pi} \sqrt{\begin{array}{l}(|H_{ext}| + H_{cry})(|H_{ext}| + M_S + H_{cry} - H_{int}) \\ +\frac{M_S}{4}(M_S - H_{int})(1 - \exp(-2|k|t_{Fe}))\end{array}}, \quad (1)$$

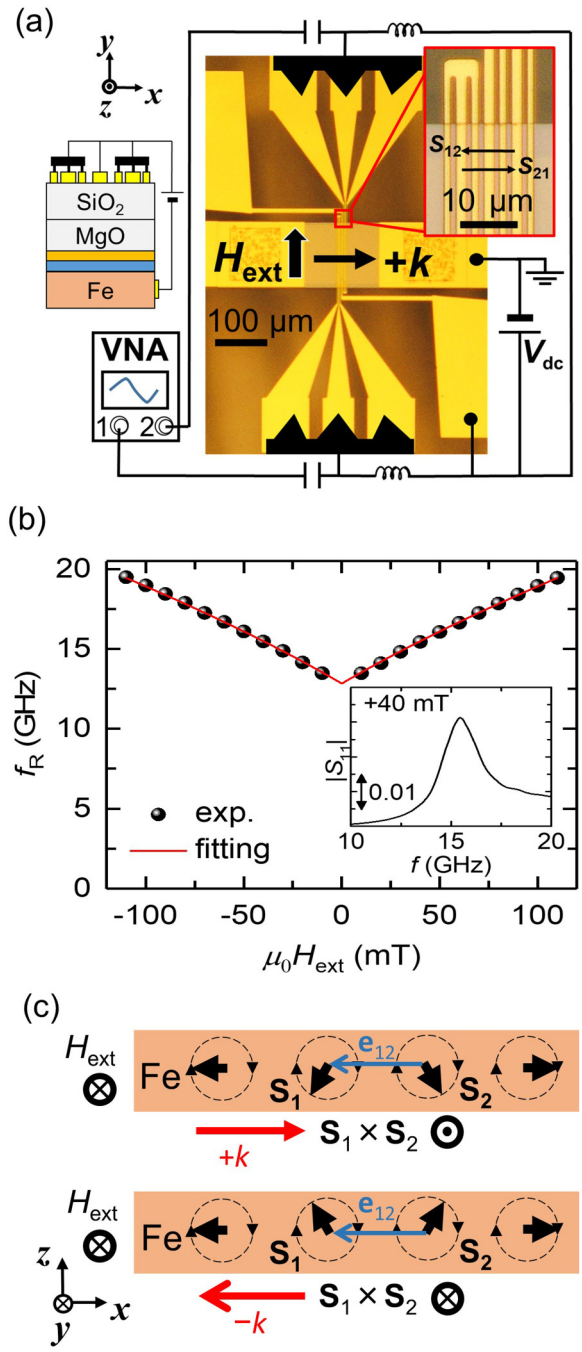

FIG. 2. (a) Optical microscope image of spin-wave device with measurement configuration schematic. An in-plane magnetic field (H_{ext} in the y direction) is applied to excite magnetostatic surface spin waves. The k vector of the MSSW is parallel to the x direction. A VNA is connected to two microscale antennas to excite and detect the spin waves. An electric field (z direction) is applied to the ferromagnetic layer through the MgO/SiO_2 dielectrics when a bias voltage (V_{dc}) is applied to the two antennas and gate electrode. (b) The magnetic-field dependence of the spin-wave resonant frequency (f_R) of Fe/Co (0.52 nm)/Pd (0.19 nm), determined from the peak position of the S_{11} signal. The red curve shows fitting [Eq. (1)]. (c) Directional dependence of MSSW propagation. MSSW with $+k$ and $-k$ correspond to signals from VNA of S_{21} and S_{12}, respectively. Black arrows indicate the spin direction; circles represent the precessional motion of the spin.

where γ_0 is the gyromagnetic ratio of Fe [$-\gamma_0/2\pi = 2.94 \times 10^{10} 1/(\mathrm{T \cdot s})$], μ_0 is the permeability of vacuum ($4\pi \times 10^{-7}\,\mathrm{H\,m^{-1}}$), M_S is the saturation magnetization of the bulk Fe ($\mu_0 M_S = 2.16\,\mathrm{T}$), k is the wave number ($1.2\,\mu\mathrm{m}^{-1}$) determined by the waveguide design, and t_{Fe} is the thickness of the Fe layer (20 nm). While the interfacial property $\mu_0 H_{int}$ might be sensitive to Co and Pd insertion, the bulk physical properties, i.e., γ_0, M_S, and t_{Fe}, are assumed to be constant. This is because the thicknesses of the inserted Co and Pd layers (< 1 nm) are much smaller than that of the Fe layer (20 nm). $\mu_0 H_{int}$ is correlated to the perpendicular magnetic anisotropy energy, K_i, and is expressed as $K_i = \mu_0 M_S t_{Fe} H_{int}/2$. The S_{11} spectrum includes the excitation of MSSWs in both the $+k$ and $-k$ directions; therefore, the spectrum may show splitting from the iDMI contribution [25,26]. However, in Fig. 2(b), it is difficult to confirm splitting in the S_{11} spectrum. The original iDMI is small because of the relatively thick ferromagnetic layer (~20 nm); therefore, the possible peak split caused by the iDMI energy would be much smaller than the linewidth of the spectra. For this reason, the iDMI term was neglected in Eq. (1).

To characterize the VCMA and iDMI changes, spin-wave spectroscopy with a modulation technique [20] was implemented. We averaged 600 individual spectra of the S_{21} and S_{12} propagation signals under an applied bias voltage. Figure 2(c) illustrates the directional dependence of MSSW propagation. It shows that MSSWs with different k directions possess different vector spin chiralities. This nonreciprocal property of the MSSW reflects the iDMI in the system. The iDMI energy can be calculated from the difference between the S_{21} and S_{12} signals, which correspond to the $+k$ and $-k$ propagation directions, respectively.

III. RESULTS AND DISCUSSION

The interfacial perpendicular magnetic anisotropy field ($\mu_0 H_{int}$) in the Fe/Co/Pd/MgO multilayers for various configurations of materials and thicknesses is summarized in Fig. 3. In Fig. 3, the multilayer is not postannealed. In the inset

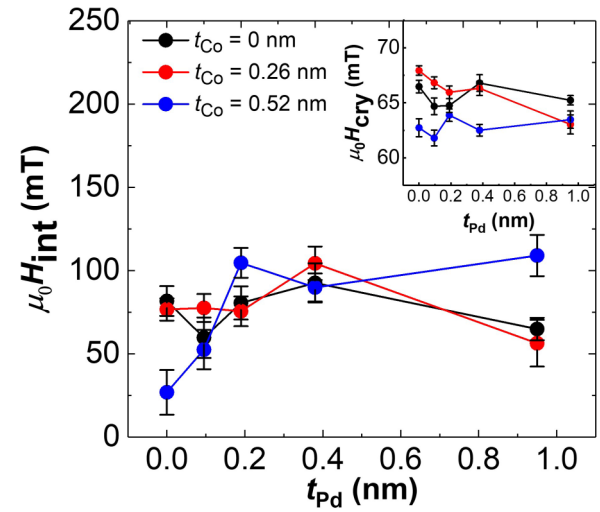

FIG. 3. Interfacial perpendicular magnetic anisotropy field ($\mu_0 H_{int}$) as a function of Pd thickness (t_{Pd}) for various thicknesses of Co (t_{Co}). Inset graph shows the crystalline anisotropy field ($\mu_0 H_{cry}$).

graph, a slight change in the $\mu_0 H_{cry}$ value from the Co and Pd insertion is observed; the value ranges within 7% of the value for the Fe/MgO sample ($\mu_0 H_{cry} = 66.4 \pm 0.6$ mT). However, $\mu_0 H_{int}$ shows significant changes for different interfaces. For the Fe/Co/MgO system ($t_{Pd} = 0$ nm), increasing t_{Co} decreases $\mu_0 H_{int}$, implying that the perpendicular magnetic anisotropy (PMA) in the system is decreased by the presence of Co. Such behavior is consistent with a previous report [27] in which the PMA at an Fe/MgO interface was greater than that at Co/MgO.

The Pd thickness dependence is discussed as follows. A few monolayers of interfacial Pd atoms with ferromagnetic metals should be spin polarized because of ferromagnetic proximity-induced effects [28,29]. In this regard, in the relatively thin region ($t_{Pd} < 0.4$ nm), Pd atoms at the interface of MgO should be ferromagnetic and the interfacial PMA energy should come from the Pd/MgO interface. In contrast, in the relatively thick region (~1 nm), Pd atoms at the interface of MgO should be paramagnetic and the interfacial PMA energy should not come from the Pd/MgO interface but from the Fe/Pd interface. For Fe/Pd/MgO ($t_{Co} = 0$ nm), $\mu_0 H_{int}$ is almost constant as t_{Pd} increases, suggesting that the PMA at the Fe/MgO ($t_{Pd} = 0$ nm), Pd/MgO ($t_{Pd} \sim 0.2$ nm), and Fe/Pd ($t_{Pd} \sim 1$ nm) interfaces are almost identical to each other. For thick Co ($t_{Co} = 0.52$ nm), the interface can be regarded as Co/Pd/MgO. $\mu_0 H_{int}$ is increased from 25 mT (Co/MgO, $t_{Pd} = 0$ nm) to ~100 mT ($t_{Pd} > 0.2$ nm), suggesting that the PMA values of the Pd/MgO ($t_{Pd} = 0$ nm) and Co/Pd ($t_{Pd} \sim 1$ nm) interfaces are comparable, but are larger than that of the Co/MgO interface ($t_{Pd} = 0$ nm). For the 0.26-nm Co, the interface may be mixed Co-Fe/Pd/MgO with intermediate PMA values. The error bars of $\mu_0 H_{int}$ and $\mu_0 H_{cry}$, originally determined from fitting using Eq. (1), represent the standard deviation obtained by the root-mean-square method.

The voltage-induced effect is now discussed. As mentioned earlier, the analyses of the VCMA and iDMI changes were conducted through the spin-wave propagation signals (S_{21} and S_{12}). Figures 4(a) and 4(b) show typical spectra of the real parts of S_{21} and S_{12}, respectively, for the Fe/Co (0.52 nm)/Pd (0.19 nm)/MgO sample taken at $V_{dc} = 0$ V and $\mu_0 H_{ext} = 40$ mT. Afterward, a bias voltage reaching 5 V is applied. Solid lines in Figs. 4(c) and 4(d) show the subtracted signal $\Delta\mathrm{Re}[S_{21(12)}] = \mathrm{Re}[S_{21(12)}(5\mathrm{V})] - \mathrm{Re}[S_{21(12)}(0\,\mathrm{V})]$, indicating that the signal is modulated by the bias voltage. We define this modulation as the voltage-induced frequency shift (δf_R) and estimate its value by fitting to the function expressed as

$$\Delta\mathrm{Re}[S_{21(12)}] = -\delta f_{21(12)} \frac{d\mathrm{Re}[S_{21(12)}]}{df}, \tag{2}$$

where $d\mathrm{Re}[S_{21(12)}]/df$ is the numerical differentiation of the experimentally obtained $S_{21(12)}$ spectrum. The intensity difference between S_{21} and S_{12} observed in Figs. 4(a) and 4(b) is attributed to the mismatch of spatial rotation of the radio-frequency field and the MSSW [30]. Figure 4(e) shows the voltage-induced frequency shift (δf_R) as a function of the bias voltage (V_{dc}). The solid and dashed lines represent δf_{21} and δf_{12}, respectively. These have similar tendencies, showing increases as functions of V_{dc}, which arise from the VCMA effect. Moreover, a small but significant difference appears

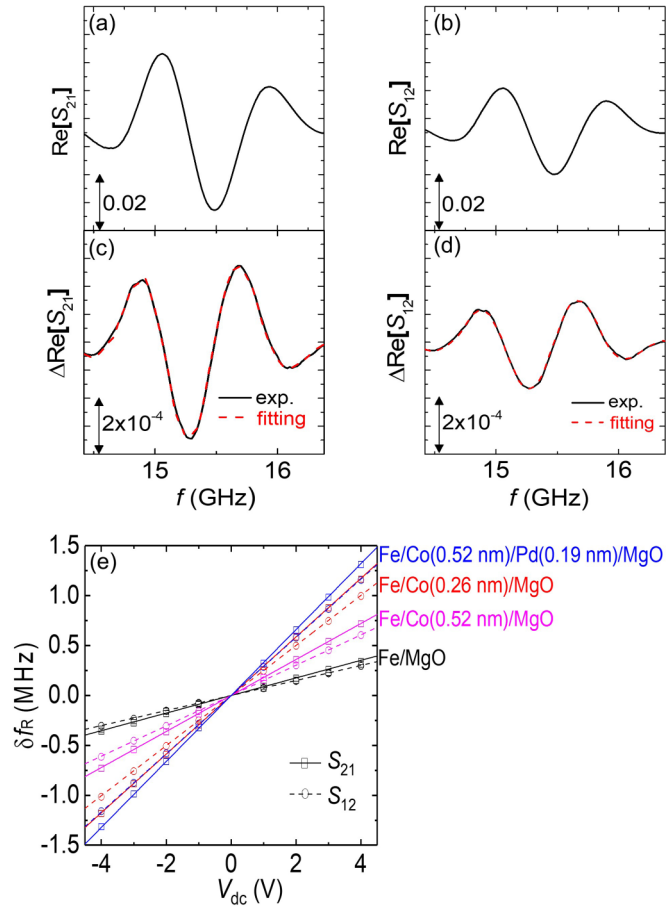

FIG. 4. (a), (b) Typical spin-wave propagation signals of Fe/Co (0.52 nm)/Pd (0.19 nm)/MgO in $+k(S_{21})$ and $-k(S_{12})$ directions under zero bias voltage ($V_{dc} = 0$ V) measured under $\mu_0 H_{ext} = 40$ mT. (c), (d) Typical voltage-induced change in the spin-wave signals, where the S_{21} and S_{12} taken at 0 V are subtracted from those taken at 5 V. The red curve shows fitting [Eq. (2)]. (e) Typical resonant frequency shifts (δf_R) as functions of V_{dc}.

between the slopes of δf_{21} and δf_{12}, which originates from the voltage-induced iDMI change in the system. Figure 4(e) shows the frequency shifts for several insertion thicknesses. A linear relation is observed between δf and V_{dc}. We obtain the highest slope of $\delta f_{21} = 0.329 \pm 0.001$ MHz/V for Fe/Co (0.52 nm)/Pd (0.19 nm)/MgO; it is approximately 3.5 times larger than the slope obtained with Fe/MgO. This is discussed later in detail.

The VCMA magnitude is defined as the change of the interfacial perpendicular magnetic anisotropy upon voltage application. For a propagating spin wave, the resonant frequency (f_R) can be expressed as the contributions of the anisotropy and iDMI terms [20,25]:

$$f_R = -\frac{\gamma_0 \mu_0}{2\pi} \sqrt{\begin{aligned}&(|H_{ext}| + H_{cry})(|H_{ext}| + M_S + H_{cry} - H_{int}(V_{dc})) \\ &+ \frac{M_S}{4}(M_S - H_{int}(V_{dc}))(1 - e(-2|k|t_{Fe}))\end{aligned}} \mp \frac{\gamma_0}{\pi} \frac{D(V_{dc})k}{M_S}, \tag{3}$$

where D is the iDMI contribution and $\mp$ denotes the magnetic-field direction. When a bias voltage modulates $H_{\rm int}$, that is, under the VCMA effect, $f_{\rm R}$ should be shifted. From the shift of $f_{\rm R}(\delta f)$, we can calculate the VCMA efficiency from Eq. (3) expressed as follows:

$$\xi_{\rm VCMA} = -\frac{M_{\rm S}t_{\rm Fe}}{\mu_0 E_{\rm MgO}} \frac{\left(\frac{2\pi}{\gamma_0}\right)^2 f_{\rm R}\left(\frac{\delta f_{21}+\delta f_{12}}{2}\right)}{\left(H_{\rm ext}+H_{\rm cry}+\frac{M_{\rm S}}{4}(1-e^{-2kt_{\rm Fe}})\right)}, \quad (4)$$

where $E_{\rm MgO} = 0.008\,{\rm nm}^{-1} \times V_{\rm dc}$ is the electric field in the MgO layer. Here, we modeled the sample as two capacitors in series where the dielectric constants of SiO_2 and MgO are 3.9 and 9.6, respectively. The polarity of the voltage is defined as positive (or negative) when electrons (or holes) are induced at the Fe/MgO interface. Moreover, we can calculate the voltage-induced iDMI change by considering the directional dependence of δf:

$$\xi_{i\rm DMI} = -\frac{\pi}{\gamma_0}\frac{M_{\rm S}}{E_{\rm MgO}k}\left(\frac{\delta f_{21}-\delta f_{12}}{2}\right), \quad (5)$$

equation (5) can be derived from Eq. (3). For both VCMA and iDMI change, the coefficients are determined by the interface and are independent of the bulk properties. The fitting coefficient for the VCMA $(\delta f_{21}+\delta f_{12})$ and iDMI change $(\delta f_{21}-\delta f_{12})$ are not interdependent. In this study, the error bar for the changes in VCMA and iDMI (Fig. 6) are determined from the standard error of the $\delta f_{\rm R}$ vs $V_{\rm dc}$ slope [Fig. 4(e)], which can be expressed as

$$\varepsilon_{\delta f_{\rm R}/V_{\rm dc}} = \frac{\sqrt{\sum_{i=1}^{n}\left(\delta f_{{\rm R}_i}-\delta\hat{f}_{{\rm R}_i}\right)^2/(n-1)}}{\sqrt{\sum_{i=1}^{n}\left(V_{{\rm dc}_i}-\overline{V}_{\rm dc}\right)^2}}, \quad (6)$$

where n is the number of data points and $\delta f_{\rm R}-\delta\hat{f}_{\rm R}$ denotes the residue of $\delta f_{\rm R}$.

The results of voltage-induced effects, that is, the changes in VCMA and iDMI for as-grown samples, are shown in Fig. 5 as functions of $t_{\rm Pd}$. The interfacial Pd atoms with ferromagnetic metals are expected to be spin polarized because of ferromagnetic proximity-induced effects [28,29]. First, we discuss the VCMA results shown in Fig. 5(a). The VCMA tends to decrease as $t_{\rm Pd}$ is increased in Fe/MgO. If the VCMA coefficients at the Fe/MgO and Pd/MgO interfaces with proximity-induced spin polarization from Fe are opposite to each other, such VCMA decrease with increasing $t_{\rm Pd}$ can be explained. Similarly, it has previously been reported that $L1_0$-FePd/MgO shows a positive VCMA effect [31], which is the same VCMA polarity as that of Fe/Pd/MgO obtained in this study. Compared to the Fe/MgO interface, the VCMA at the Fe/Co (0.52 nm)/MgO interface is increased with increasing $t_{\rm Pd}$. The highest VCMA efficiency of $-180\,{\rm fJ/Vm}$ is obtained at $t_{\rm Pd} = 0.19\,{\rm nm}$. This shows that the Pd/MgO interface with proximity-induced spin polarization from Co has a larger VCMA than the interface of Co/MgO; both VCMAs have the same polarity. Therefore, Pd insertion contributes constructively to the VCMA effect. Interestingly, VCMA effect at the Pd/MgO interface with proximity-induced spin polarization from Fe and that from Co have opposite signs. The tendency for the VCMA effect

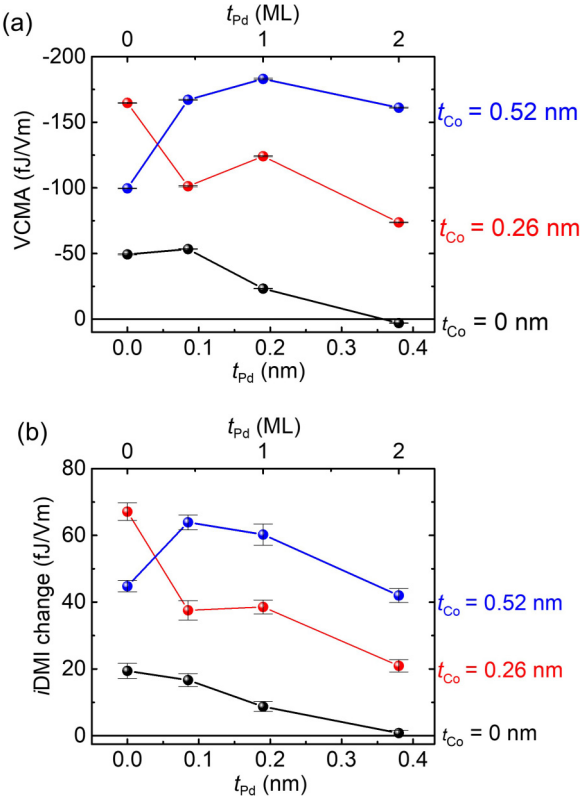

FIG. 5. The Pd thickness ($t_{\rm Pd}$) dependence of (a) voltage-controlled magnetic anisotropy [Eq. (4)] and (b) voltage-induced interfacial Dzyaloshinskii-Moriya interaction [Eq. (5)] change for the as-grown samples. Black plots represent the Fe/MgO samples.

in the Fe/Co (0.26 nm)/Pd/MgO interface is between that in Fe/Pd/MgO and Fe/Co (0.52 nm)/Pd/MgO.

It was reported that voltage-induced changes in the orbital magnetic moment in the Co/MgO system [32] were larger than those in the Fe/MgO system [33,34]. Because the orbital magnetic moment mechanism explains the VCMA effect in $3d$ transition metals [32,35], the observed larger VCMA in the Co/MgO system than that in the Fe/MgO system in this study is consistent with the reported larger orbital magnetic moment change. Notably, the voltage-induced change in orbital magnetic moment is estimated to be only 0.1% of the total magnetic moment [32]. Thus, its influences on magnetization change are negligibly small. With Pd insertion, the situation might be different. For the Fe(Co)/Pd/MgO system, the interfacial Pd metal with induced spin polarization should explain the VCMA. Because of the strong electrostatic screening effect, the electric field is only applied to atoms interfacing with MgO in ferromagnetic materials [15,32]. The larger VCMA in the Pd/MgO system is attributed to the large spin-orbit interaction coefficient in Pd and/or the existence of the electric quadrupole mechanism, in addition to the orbital magnetic moment mechanism [15]. The source of the difference in the VCMA polarities between the Co/Pd/MgO and Fe/Pd/MgO systems remains an open question. For Fe/Co (0.26 nm)/MgO, the VCMA effect ($-165\,{\rm fJ/Vm}$) is larger than that of Fe/Co (0.26 nm)/MgO. This may be because of the larger magnetic moment of Co in the Fe/Co (0.26 nm)/MgO system than that

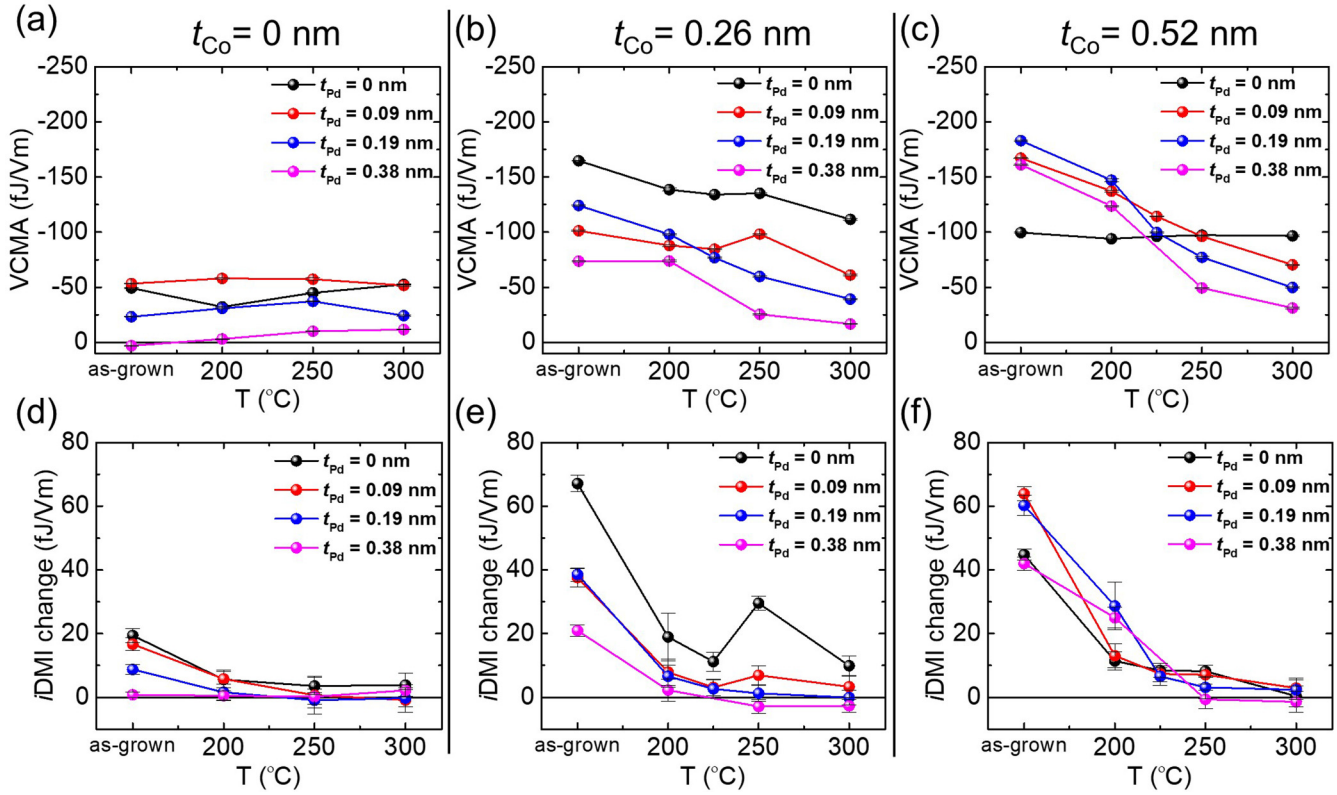

FIG. 6. VCMA [Eq. (4)] and *i*DMI changes [Eq. (5)] as functions of postannealed temperatures (T). Co thicknesses of (a), (d) 0 nm; (b), (e) 0.26 nm; and (c), (f) 0.52 nm, respectively.

in the Fe/Co (0.52 nm)/MgO system [32]. Because the VCMA efficiency is proportional to the orbital magnetic moment change in such a system, a larger magnetic moment can induce a larger VCMA efficiency. For Pd insertion in the Fe/Co (0.26 nm)/MgO sample, the interface with MgO may be mixed FeCo, with VCMA contributions from both Co/Pd/MgO and Fe/Pd/MgO.

Second, we discuss the voltage-induced *i*DMI change for the as-grown multilayer samples. The *i*DMI energy should exist on the top and bottom layers attached to the ferromagnetic metals. In our study, the voltage-induced *i*DMI change should be attributed only to the top side, which is attached to the MgO. This is because the bias electric field is applied only to interfacial atoms around MgO [15,32]. Figure 5(b) shows the *i*DMI change for the as-deposited samples. It shows that the Co/MgO interface has a larger *i*DMI change than that of Fe/MgO. Moreover, thin Pd insertion in the Co (0.52 nm)/MgO system enhances the *i*DMI change.

As discussed for the VCMA effect, it was reported that voltage-induced changes in orbital magnetic moment in Co/MgO [32] were larger than those in Fe/MgO [33,34]. This strongly suggests that the voltage-induced orbital angular momentum is larger at the Co/MgO interface. Because *i*DMI is strongly related to the orbital angular momentum in ferromagnetic materials [36,37], the *i*DMI change in Co/MgO is larger than that in Fe/MgO. In Fig. 5(b), the *i*DMI change is enhanced by Pd insertion, which is probably mediated by the large spin-orbit interaction coefficient of Pd. In this work, the maximum *i*DMI change of 65 fJ/Vm is obtained in the Fe/Co (0.26 nm)/MgO system. Because the *i*DMI is inversely proportional to the ferromagnetic layer thickness [38,39], the *i*DMI change of 65 fJ/Vm corresponds to the *i*DMI energy density change of $\sim$1.3 mJ/m^2. when the 1-nm-thick ferromagnetic layer and 1-V/nm electric field are employed in MgO. If we use MTJ devices, such conditions can be easily prepared. Therefore, it should be noted that the voltage-induced *i*DMI change is large enough to stabilize and destabilize chiral magnetic structures such as skyrmion states [40].

Finally, the postannealing influence on VCMA and *i*DMI change is discussed. Figures 6(a)–6(c) show the VCMA values as functions of the annealing temperature for three different Co thicknesses. For the Fe/MgO and Co (0.52 nm)/MgO interfaces, the impact of postannealing is not significant. This suggests that postannealing does not significantly change the materials interfacing with MgO. However, the VCMA in Fe/Co (0.26 nm)/MgO shows a monotonic decrease with postannealing. This is probably because postannealing enhances the alloying of Fe and Co at the interface with MgO.

When Pd is introduced at the Fe/MgO and Co/MgO interfaces, the situations differ. Postannealing slightly increases the VCMA in Fe/Pd/MgO [Fig. 6(a)] and significantly decreases the VCMA in Co/Pd/MgO [Figs. 6(b) and 6(c)]. For Fe/Pd/MgO, because postannealing enhances the Pd diffusion into Fe, we may expect the influence of Pd/MgO on VCMA to decrease. For Fe/Co/Pd/MgO, the decrease of VCMA can be attributed to the change in the chemical order in the Co-Pd alloy located at the interface with MgO. Recently, it was reported that an FeIr alloy/MgO structure showed the large VCMA of -320 fJ/Vm (Ref. [16]), suggesting that a change

in the chemical order around the interface with MgO was effective in enhancing the VCMA. This is because changes in the chemical order affect both contributions from the VCMA mechanisms, that is, orbital magnetic moment and electric-quadrupole mechanisms [15,19]. Apart from this, our results show that VCMA in the FePd alloy/MgO system is slightly higher than that in the Fe/Pd/MgO system, whereas that in the CoPd alloy/MgO system is much smaller than that in the Co/Pd/MgO system. Therefore, the chemical order of 1, that is, the layered multilayer realized in the as-deposited sample, is the best condition for the VCMA effect in the Co-Pd/MgO systems.

Figures 6(d)–d(f) show the iDMI change for $t_{\mathrm{Co}} = 0$, 0.26, and 0.52 nm as functions of the postannealed temperature. The iDMI change decreases as the annealing temperature increases for all systems. To discuss the iDMI change, the following two models of Rashba [41] and spin current [42] can be employed. As discussed previously [21,39,43], the Rashba model is more applicable for ferromagnetic metals with insulating dielectric layers, such as MgO. For both models, iDMI cannot be explained by either on-site (intra-atomic) magnetic properties, as the VCMA effect can, or interatomic ones. A postannealing induces intermixing around the interface with MgO. Therefore, postannealing changes the on-site magnetic properties because of the replacement of the materials forming interfaces with MgO. For this reason, the tendencies of VCMA and iDMI changes should be similar, which is experimentally observed for the Pd-inserted samples. However, the tendencies for the changes in VCMA and iDMI are very different for the case of Fe/MgO and Co/MgO. The iDMI change is sensitive to postannealing, while the VCMA effect is not. This strongly suggests that the iDMI change is sensitive to slight changes of the in-plane lattice constant and/or dislocations around the interface with MgO, which is not the case for the VCMA effect, governed only by on-site magnetic properties. Similarly, it was reported that postannealing decreased iDMI in $\mathrm{Pt/Co/AlO}_x$ and $\mathrm{Pt/CoFeB/AlO}_x$ systems [44].

IV. SUMMARY

The influence of Co and Pd monolayer insertions at Fe/MgO interfaces on voltage-controlled magnetic anisotropy and voltage-induced Dzyaloshinskii-Moriya interaction change was investigated. As compared with Fe/MgO, an opposite sign of VCMA efficiency was obtained in Fe/Pd/MgO, while in Co/MgO a larger VCMA efficiency was obtained. Moreover, Pd insertion at the Co/MgO interface enhanced the VCMA efficiency. We obtained the largest VCMA efficiency of $-180\,\mathrm{fJ/Vm}$ in the Fe/Co/Pd system. Moreover, the high iDMI change of $65\,\mathrm{fJ/Vm}$ was obtained in Fe/Co/MgO. For the Fe/Co/Pd system, the postannealing process monotonically reduced VCMA and iDMI change with increasing temperature. Therefore, we concluded that layered multilayers, rather than alloys, provide the best conditions for manipulating VCMA and iDMI in CoPd/MgO systems. These findings could provide leads in the development of voltage-driven spintronic devices.

ACKNOWLEDGMENTS

We thank S. Kim of Kyoto University and K. Masuda and Y. Miura of NIMS for fruitful discussion. A part of this work was supported by JSPS KAKENHI (Grants No. JP18H03880 and No. JP26103002), TEPCO Memorial Foundation, and the ImPACT program. J.C. was supported by Postdoctoral Fellowship for Foreign Researchers program (Grant No. P16362) of Japan Society for the Promotion of Science (JSPS). J.S. thanks the Indonesia Endowment Fund for Education (LPDP) for the financial support during the doctoral study.

[1] J. A. Katine, F. J. Albert, R. A. Buhrman, E. B. Myers, and D. C. Ralph, Phys. Rev. Lett. **84**, 3149 (2000).
[2] K. Ando, S. Fujita, J. Ito, S. Yuasa, Y. Suzuki, Y. Nakatani, T. Miyazaki, and H. Yoda, J. Appl. Phys. **115**, 172607 (2014).
[3] R. Landauer, IBM J. Res. Dev. **5**, 183 (1961).
[4] M. Weisheit, S. Fahler, A. Marty, Y. Souche, C. Poinsignon, and D. Givord, Science **315**, 349 (2007).
[5] T. Maruyama, Y. Shiota, T. Nozaki, K. Ohta, N. Toda, M. Mizuguchi, A. Tulapurkar, T. Shinjo, M. Shiraishi, S. Mizukami, Y. Ando, and Y. Suzuki, Nat. Nanotechnol. **4**, 158 (2009).
[6] P. K. Amiri, J. G. Alzate, X. Q. Cai, F. Ebrahimi, Q. Hu, K. Wong, C. Grezes, H. Lee, G. Yu, X. Li, M. Akyol, Q. Shao, J. A. Katine, J. Langer, B. Ocker, and K. L. Wang, IEEE Trans. Magn. **51**(11), 3401507 (2015).
[7] T. Nozaki, Y. Shiota, M. Shiraishi, T. Shinjo, and Y. Suzuki, Appl. Phys. Lett. **96**, 022506 (2010).
[8] Y. Shiota, T. Nozaki, F. Bonell, S. Murakami, T. Shinjo, and Y. Suzuki, Nat. Mater. **11**, 39 (2012).
[9] S. Kanai, M. Yamanouchi, S. Ikeda, Y. Nakatani, F. Matsukura, and H. Ohno, Appl. Phys. Lett. **101**, 122403 (2012).
[10] C. Grezes, F. Ebrahimi, J. G. Alzate, X. Cai, J. A. Katine, J. Langer, B. Ocker, P. K. Amiri, and K. L. Wang, Appl. Phys. Lett. **108**, 012403 (2016).
[11] T. Nozaki, Y. Shiota, S. Miwa, S. Murakami, F. Bonell, S. Ishibashi, H. Kubota, K. Yakushiji, T. Saruya. A. Fukushima, S. Yuasa, T. Shinjo, and Y. Suzuki, Nat. Phys. **8**, 492 (2012).
[12] J. Zhu, J. A. Katine, G. E. Rowlands, Y.-J. Chen, Z. Duan, J. G. Alzate, P. Upadhyaya, J. Langer, P. K. Amiri, K. L. Wang, and I-. N. Krivototov, Phy. Rev. Lett. **108**, 197203 (2012).
[13] M. Tsujikawa and T. Oda, Phys. Rev. Lett. **102**, 247203 (2009).
[14] K. Nakamura, T. Nomura, A. M. Pradipto, K. Nawa, T. Akiyama, and T. Ito, J. Magn. Magn. Mater. **429**, 214 (2017).
[15] S. Miwa, M. Suzuki, M. Tsujikawa, K. Matsuda, T. Nozaki, K. Tanaka, T. Tsukahara, K. Nawaoka, M. Goto, Y. Kotani, T. Ohkubo, F. Bonell, E. Tamura, K. Hono, T. Nakamura, M. Shirai, S. Yuasa, and Y. Suzuki, Nat. Commun. **8**, 15848 (2017).
[16] T. Nozaki, A. Kozioł-Rachwał, M. Tsujikawa, Y. Shiota, X. Xu, T. Ohkubo, T. Tsukahara, S. Miwa, M. Suzuki, S. Tamaru, H. Kubota, A. Fukushima, K. Hono, M. Shirai, Y. Suzuki, and S. Yuasa, NPG Asia Mater. **9**, e451 (2017).

[17] Y. Hibino, T. Koyama, A. Obinata, K. Miwa, S. Ono, and D. Chiba, Appl. Phys. Express **8**, 113002 (2015).
[18] Y. Hibino, T. Koyama, A. Obinata, T. Hirai, K. Miwa, S. Ono, F. Matsukura, H. Ohno, and D. Chiba, Appl. Phys. Lett. **109**, 082403 (2016).
[19] P. Kamp, A. Marty, B. Gilles, R. Hoffmann, S. Marchesini, M. Belakhovsky, C. Boeglin, H. A. Dürr, S. S. Dhesi, G. vanderLaan, and A. Rogalev, Phys. Rev. B **59**, 1105 (1999).
[20] K. Nawaoka, S. Miwa, Y. Shiota, N. Mizuochi, and Y. Suzuki, Appl. Phys. Express **8**, 063004 (2015).
[21] H. Yang, O. Boulle, V. Cros, A. Fert, and M. Chshiev, Sci. Rep. **8**, 12356 (2018).
[22] H. Imamura, T. Nozaki, S. Yuasa, and Y. Suzuki, The 41st Annual Conference on MAGNETICS in Japan, 20aD-5 (2017) (unpublished).
[23] P.-J. Hsu, A. Kubetzka, A. Finco, N. Romming, and K. von Bergmann, Nat. Nanotechnol. **12**, 123 (2016).
[24] A. Kozioł-Rachwał, T. Nozaki, V. Zayets, H. Kubota, A. Fukushima, S. Yuasa, and Y. Suzuki, J. Appl. Phys. **120**, 085303 (2016).
[25] J.-H. Moon, S.-M. Seo, K.-J. Lee, K.-W. Kim, J. Ryu, H.-W. Lee, R. D. McMichael, and M. D. Stiles, Phys. Rev. B **88**, 184404 (2013).
[26] Kh. Zakeri, Y. Zhang, J. Prokop, T.-H. Chuang, N. Sakr, W. X. Tang, and J. Kirschner, Phys. Rev. Lett. **104**, 137203 (2010).
[27] H. X. Yang, M. Chshiev, B. Dieny, J. H. Lee, A. Manchon, and K. H. Shin, Phys. Rev. B. **84**, 054401 (2011).
[28] U. Gradmann and R. Bergholz, Phys. Rev. Lett. **52**, 771 (1984).
[29] F. J. A. den Broeder, H. C. Donkersloot, H. J. G. Draasima, and W. J. M. de Jonge, J. Appl. Phys. **61**, 4317 (1987).
[30] V. E. Demidov, M. P. Kostylev, K. Rott, P. Krzysteczko, G. Reiss, and S. O. Demokritov, Appl. Phys. Lett. **95**, 112509 (2009).
[31] F. Bonell, S. Murakami, Y. Shiota, T. Nozaki, T. Shinjo, and Y. Suzuki, Appl. Phys. Lett. **98**, 232510 (2011).
[32] T. Kawabe, K. Yoshikawa, M. Tsujikawa, T. Tsukahara, K. Nawaoka, Y. Kotani, K. Toyoki, M. Goto, M. Suzuki, T. Nakamura, M. Shirai, Y. Suzuki, and S. Miwa, Phys. Rev. B. **96**, 220412(R) (2017).
[33] S. Miwa, K. Matsuda, K. Tanaka, Y. Kotani, M. Goto, T. Nakamura, and Y. Suzuki. Appl. Phys. Lett. **107**, 162402 (2015).
[34] T. Tsukahara, T. Kawabe, K. Shimose, T. Furuta, R. Miyakaze, K. Nawaoka, M. Goto, T. Nozaki, S. Yuasa, Y. Kotani, K. Toyoki, M. Suzuki, T. Nakamura, Y. Suzuki, and S. Miwa, Jpn. J. Appl. Phys. **56**, 060304 (2017).
[35] P. Bruno, Phys. Rev. B **39**, 865 (1989).
[36] I. E. Dzyaloshinskii, Sov. Phys. JETP **5**, 1259 (1957).
[37] T. Moriya, Phys. Rev. **120**, 91 (1960).
[38] J. Cho, N. Kim, S. Lee, J. Kim, R. Lavrijsen, A. Solignac, Y. Yin, D. Han, N. J. J. van Hoof, H. J. M. Swagten, B. Koopmans, and C. You, Nat. Commun. **6**, 7635 (2015).
[39] H. Yang, A. Thiaville, S. Rohart, A. Fert, and M. Chshiev, Phys. Rev. Lett. **115**, 267210 (2015).
[40] S. Mühlbauer, B. Binz, F. Jonietz, C. Pfleiderer, A. Rosch, A. Neubauer, R. Georgii, and P. Böni, Science **323**, 915 (2009).
[41] A. Kundu and S. Zhang, Phys. Rev. B **92**, 094434 (2015).
[42] H. Katsura, N. Nagaosa, and A. V. Balatsky, Phys. Rev. Lett. **95**, 057205 (2005).
[43] A. Cao, X. Zhang, B. Koopmans, S. Peng, Y. Zhang, Z. Wang, S. Yan, H. Yang, and W. Zhao, Nanoscale **10**, 12062 (2018).
[44] J. Cho, N.-H. Kim, J. Jung, D.-S. Han, H. J. M. Swagten, J.-S. Kim, and C.-Y. You, IEEE Trans. Magn. **54**(6), 1500104 (2018).